Journal of
Micro/Nanolithography,
MEMS, and MOEMS

SPIEDigitalLibrary.org/jm3

Impact of the phase defect structure on an actinic dark-field blank inspection signal and wafer printability

Tsuyoshi Amano
Yukiyasu Arisawa
Tsuneo Terasawa

SPIE

Impact of the phase defect structure on an actinic dark-field blank inspection signal and wafer printability

Tsuyoshi Amano
Yukiyasu Arisawa
Tsuneo Terasawa
EUVL Infrastructure Development Center Inc.
16-1 Onogawa, Tsukuba-shi
Ibaraki-ken 305-8569, Japan
E-mail: tsuyoshi.amano@eidec.co.jp

Abstract. In extreme ultraviolet lithography, reducing the number of phase defects (PDs) on mask blanks is a critical issue because the PDs cause degradation of the printed pattern quality. To minimize the number of printable PDs, covering PDs beneath an absorber pattern is an effective way of addressing the problem. Therefore it becomes necessary to detect the PDs and pinpoint their locations by a blank inspector. In this work, a three-dimensional analysis of PDs has revealed that some PDs can grow and propagate in an angular direction away from the normal to the substrate surface. The impact of the inclination angle on the printing performance was evaluated by calculating printed pattern images using a simulator. A PD with an inclination angle of 1 deg corresponds to a 1-nanometer positional shift compared with a position defined as surface topography of a defect as observed by an atomic force microscope or by some nonactinic defect inspector. However, an actinic blank inspection (ABI) tool with high-magnification optics can pinpoint the actual location of the PDs. Covering a PD under an absorber pattern, by a shifting of the pattern based on the information of the PD's location obtained by the ABI tool, works quite well.
© *The Authors. Published by SPIE under a Creative Commons Attribution 3.0 Unported License. Distribution or reproduction of this work in whole or in part requires full attribution of the original publication, including its DOI.* [DOI: 10.1117/1.JMM.12.2.021002]

Subject terms: extreme ultraviolet; actinic blank inspection; phase defect; defect mitigation.

Paper 12077SSP received Jul. 24, 2012; revised manuscript received Nov. 7, 2012; accepted for publication Dec. 17, 2012; published online Mar. 1, 2013.

1 Introduction

The influence of phase defects (PDs) embedded in extreme ultraviolet (EUV) mask blanks on wafer printing has always been a center of attention, because it is difficult to repair the PDs after an absorber has already been deposited on a reflective multilayer.[1,2] The root cause for the PDs is the occurrence of bumps, pits, or particles on the substrate, and from where the topography of these defects propagates through the reflective multilayer during the coating process. Such structural changes in the reflective multilayer cause phase shifts in the EUV light reflected from the mask blank and produces a low intensity EUV light spot in the aerial images at the wafer plane. Several techniques to minimize the printability of PDs have been reported. One is to cover the PDs under an absorber layer by shifting the location of the device pattern during mask patterning.[3] Another is to eliminate the influence of the phase error by removing the absorber from close proximity to the PDs.[4] The absorber removal area is decided upon after measuring the size and position of PDs using an atomic force microscope (AFM) and calculating the absorber removal area using lithography simulator. As for the growth model of the PD due to the bumps on the substrate, several transmission electron microscope (TEM) images of PDs have indicated that the growth of PD from the substrate surface to the multilayer surface does not always propagate along a vertical direction. This means that multilayer surface geometry measurement using an AFM or any nonactinic defect inspector does not always identify the correct effective location of the PDs for the defect mitigation strategies of covering or compensating PDs by absorber patterning. Therefore, to efficiently cover PDs by an absorber layer, it is necessary to take into account the cross-sectional shape of PDs and to analyze their impact using high resolution actinic imaging tools like an actinic blank inspection (ABI) tool or an aerial image measurement system.[5–8] Figure 1(a) and 1(b) shows simulation of two typical PD growth examples. Some PD growth propagates in a direction perpendicular to the surface of the substrate while others propagate at an angle as it moves away from the substrate surface. The latter type will be named as "diagonal-type" PDs. Typical impacts of the vertical and diagonal-type PDs on aerial images are shown in Fig. 2(a) and 2(b). The simulated mask models are half-pitch (hp) 88 nm lines and spaces (L/S) patterns with bump-PDs (height: 5 nm, width: 50 nm, and inclination angle: 0 deg and 6 deg) to print hp 22 nm L/S on wafer. In the case of the PDs that are partially covered by absorber pattern, the diagonal-type PDs have larger impact on defect printability than the vertical-type PDs have, even when both PDs may be at the same locations on the surface of the multilayer. In this paper, the influence of the inclination angles of PD growth on the defect printability and on defect detection signal intensity of the ABI tool will be investigated.

2 Simulation Conditions

2.1 *Simulation Condition for Defect Printability*

A simulator LAIPH™ EUV Defect Printability Simulator (Luminescent Technologies) was employed in this work. The parameters for the simulations were as follows: numerical

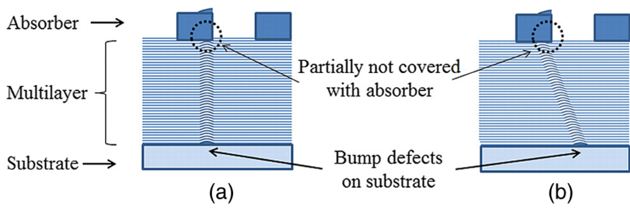

Fig. 1 Cross-sectional view of the EUVL mask pattern with: (a) vertical-type PD and (b) diagonal-type PD.

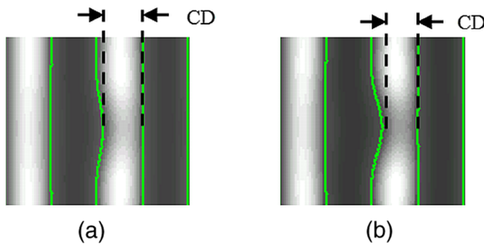

Fig. 2 Calculated aerial images of an hp 22 nm L/S pattern affected by: (a) vertical-type PD and (b) diagonal-type PD.

aperture (NA) = 0.33, sigma = 0.8 (conventional), chief-ray angle = 6 deg, demagnification = 4, and wavelength = 13.5 nm. The evaluated pattern was an hp 22 nm L/S pattern on wafer that corresponded to hp 88 nm L/S on mask parallel to the direction of the incoming of EUV light. The blank structure comprised 40 pairs of Mo/Si (Mo/Si = 2.8/4.2 nm) reflective layers with a 66 nm-thick Ta-based absorber layer grown on a 2.5 nm of Ru to serve as a cap on the Mo/Si multilayer. The defect sizes were 1, 2, 3, 4 and 5 nm in heights or depths, and 50 nm in full-width at half-maximum (FWHM). The inclination angles of the PDs were 0 deg, 3 deg, 6 deg, 9 deg, and 12 deg.

2.2 *Defining the Position and the Inclination Angle of Phase Defect, and Critical Dimension Calculation*

The positions of the PDs were defined as the peak, or valley, of the multilayer surface as illustrated in Fig. 3. The location of the PD was defined in terms of its distance from the right edge (defined as zero-position) of a line pattern illustrated in Fig. 4. The inclination angle θ was defined as the angle between a line perpendicular to the top surface of the multilayer, and an actual PD growth direction in the multilayer illustrated in Fig. 5. The defect printability was evaluated in a printed space CD calculation depicted in Fig. 2(a) and 2(b).

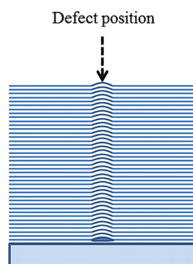

Fig. 3 Cross-sectional schematic view of PD in a multilayer.

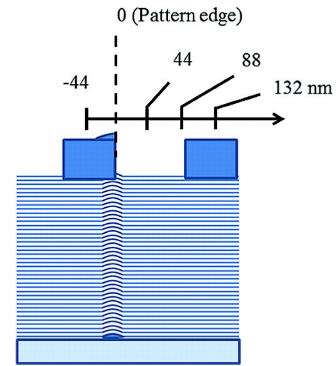

Fig. 4 Cross-sectional schematic view of PD with an absorber pattern. The scale indicates the PD position relative to the edge of the pattern.

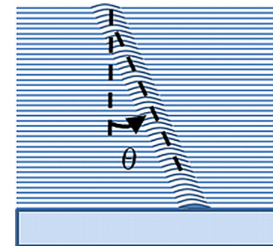

Fig. 5 Cross-sectional view of a diagonal-type PD with the inclination angle θ.

2.3 *Simulation Condition for the Analysis of Defect Detection Signal of the ABI Tool*

A simulator LAIPH™ EUV Defect Printability Simulator (Luminescent Technologies) was utilized for the calculation of the ABI tool inspection signal for detecting the diagonal-type PDs. Figure 6 shows a schematic view of the optics of the ABI tool that was developed at Selete and is being operated at EIDEC. The simulation conditions were set the same as that of the ABI tool. The parameters for the simulations were as follows: NA = 0.1/0.27 (inner/outer), pixel size at mask = 500 and 20 nm. The evaluated blank structure was Ru-capped multilayer (Ru = 2.5 nm, 40 pairs of Mo/Si = 2.8/4.2 nm). The defect sizes were set to 2, 4 and 6 nm in height (or depth) and 50 nm in FWHM. The

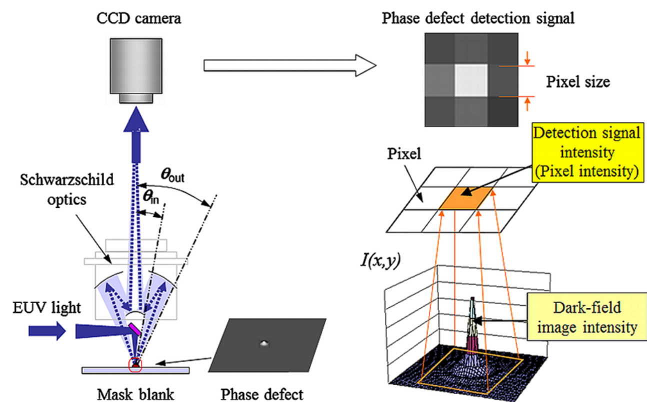

Fig. 6 Schematic view of the optics of the ABI tool with dark-field imaging and detection signal.

inclination angles of the PDs were set to 0 deg, 3 deg, 6 deg, and 9 deg.

3 Results and Discussion

3.1 *Evidence for the Existence of Diagonal-Type Phase Defect*

The ABI tool detected several native bump- and pit-PDs on the EUV reflective multilayer. Based upon the earlier analysis of the size of the PDs using AFM, a few small PDs, below 5 nm in height or depth, were prepared for TEM analysis. The analysis showed that among the PDs, some grew and propagated away from the substrate making certain angles with the substrate surface. Figure 7 shows an example of a diagonal-type PD making an inclination angle of 3.2 deg. The inclination angle of 3.2 deg causes 16 nm intensity peak position shift between the substrate surface and the multilayer surface.

3.2 *Influence of the Inclination Angle on Defect Printability*

The influences of the diagonal-type PDs on defect printability were evaluated using an hp 22 nm L/S pattern on wafer. The angle of the diagonal-type PD was set at 6 deg. The impacts of the size, position, and the inclination angle of PDs on wafer CD are summarized in Fig. 8. As expected, in the cases of both vertical-type and diagonal-type PDs, the PDs with greater heights and depths caused greater impact on wafer CD when the PDs were not covered by an absorber pattern, specifically when the location of the PD was in the range of 0 to 88 nm. To clarify the CD difference between the diagonal-type PD impact and vertical-type PD impact on wafer CD, parameters defined as delta CDs (dCD = CD[6 deg] − CD[0 deg]) were calculated and are illustrated in Fig. 9. The results indicate that the diagonal-type bump-PD or pit-PD at around the 0-nm position cause larger impact on defect printability than that of the vertical-type PD. On the other hand, the vertical-type PDs at around 88 nm in position have more impact on the printing than the diagonal-type PDs have. The reason is discussed in Sec. 3.4.

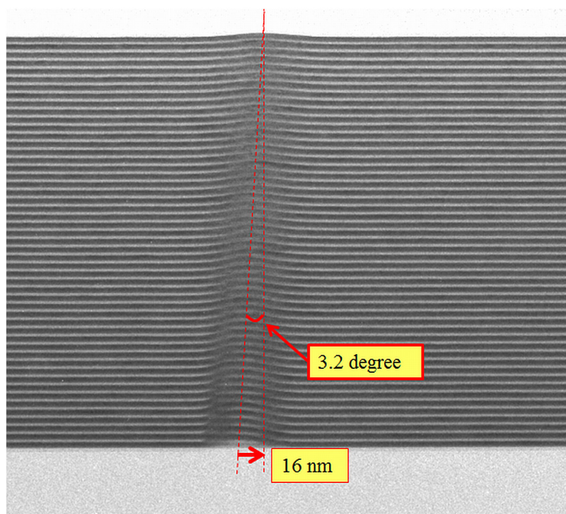

Fig. 7 TEM image of a diagonal-type native PD detected by the ABI tool.

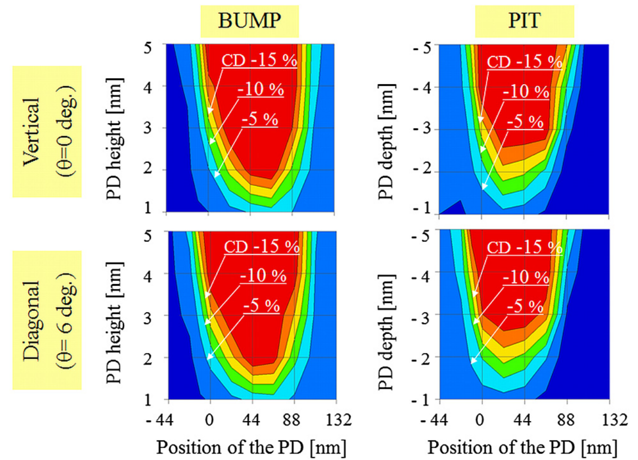

Fig. 8 Simulated CD variations as a function of the defect height or depth, position, and inclination angle. The percentage values mean CD errors of printed space pattern.

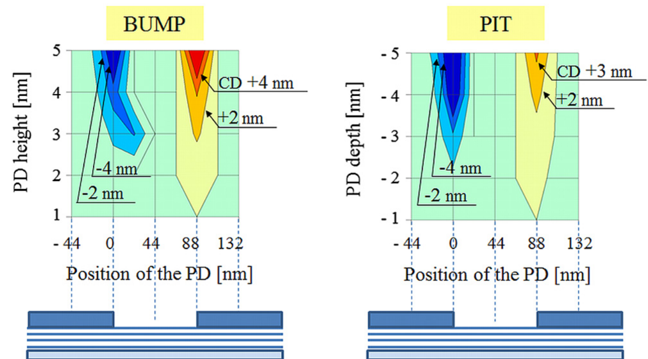

Fig. 9 CD differences between diagonal-type and vertical-type PDs.

3.3 *Influence of the Inclination Angle of Diagonal-Type PD on Printed CD*

The PD model was set to a 4-nm-high and 50-nm-wide bump with its inclination angles of 0 deg, 3 deg, 6 deg, 9 deg, and 12 deg in hp 88 nm L/S patterns at mask. The positions of the PDs relative to the absorber pattern edge were −44 nm (line center model) and −11 nm (partially covered model), as shown in Fig. 10(a) and 10(b). The calculated CDs as a function of inclination angle are shown in Fig. 11. When the top

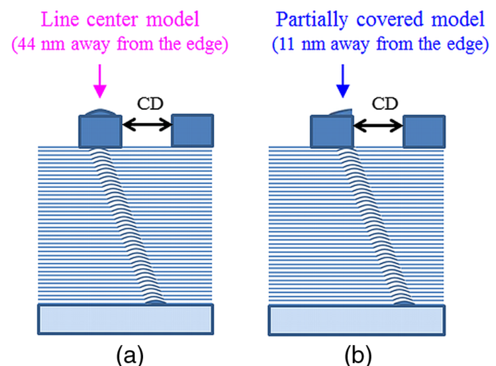

Fig. 10 Schematic view of the PD's position for (a) line center model and (b) partially covered model.

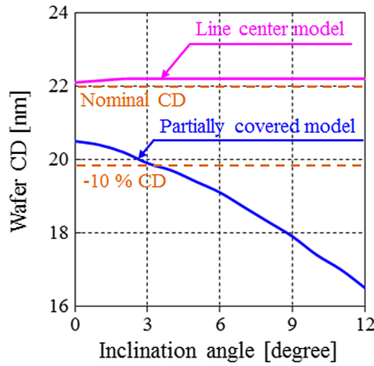

Fig. 11 Influence of the inclination angle of PDs on wafer space-CDs for two PD models. The target wafer space-CDs are 22 nm.

of the PD is completely covered by the absorber pattern, the defect printability is negligibly small even when the PD's inclined angles are in the range from 0 deg to 12 deg. However, the impact of the inclination angle on wafer CD is significant under the condition where the surface of PD is partially covered by the absorber pattern. The printed CD error could go beyond 10% when the inclination angle exceeds 3 deg while the CD error would be less than 10% if the inclination angle was zero.

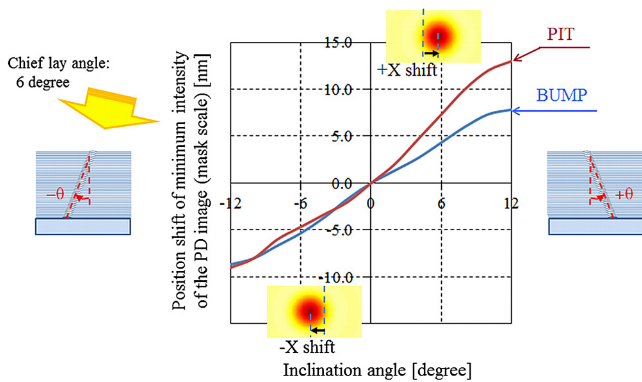

Fig. 12 Relationship between inclination angle of bump-PD and pit-PD, and position shift of minimum intensity of the PD image. The exposure condition is NA = 0.33 and a coherence factor of sigma = 0.8 (conventional).

3.4 *Inclination Angle Versus Position Shift of Minimum Intensity of PD Image, and Defect Mitigation Strategy by Shifting Absorber Pattern*

The difference between the printed CD affected by vertical-type PD and that affected by diagonal-type PD is explained by a simple model, without the absorber pattern. Figure 12 represents a relationship between the inclination angle of bump-PDs and pit-PDs (4 nm in height or depth, and 50 nm in width), and position shift of minimum intensity of the PD images on mask scale under the illumination with a chief ray angle of 6 deg. The result obviously shows that the inclination angle causes a position shift of the minimum intensity of PD image (bump-defect: 0.7 to 0.8 nm/ deg, pit-defect: 0.8 to 1.2 nm/ deg). Therefore, defect mitigation by shifting the absorber layer should be performed while taking into consideration this position shift of the PD images. To verify the effectiveness of the absorber pattern shifting method to mitigate the printable PDs while considering the inclination angle of PD, three models were designed, that involved an hp 88 nm L/S pattern and PDs with several inclination angles; defect printability was evaluated as shown in Fig. 13. Here, the designed PD is 4 nm in height, 50 nm in width, and 0 deg or 6 deg in its inclination angle. Model 1 represents a basic model where the position of PD is −11 nm, and the inclination angle is 0 deg. The calculated wafer CD is 20.3 nm (7.7% of CD error). Model 2 shows diagonal-type PD with an inclination angle of 6 deg where a relationship between the absorber pattern position and the position of the top of PD is same as that of model 1. The calculated CD is 18.9 nm (14.1% of CD error). From the calculation results shown in Fig. 12, a bump PD with 6 deg inclination corresponds to a shift in the vertical-type PD's position by about 5 nm. Therefore, in Model 3, the absorber pattern was shifted 5 nm along with the direction of PD's position shift. The calculated CD was well matched with Model 1, as expected, where the CD was 20.2 nm (8.2% of CD error). These results show that identifying the value of the position shift of a PD while considering the inclination angle is important for defect mitigation by shifting the absorber pattern.

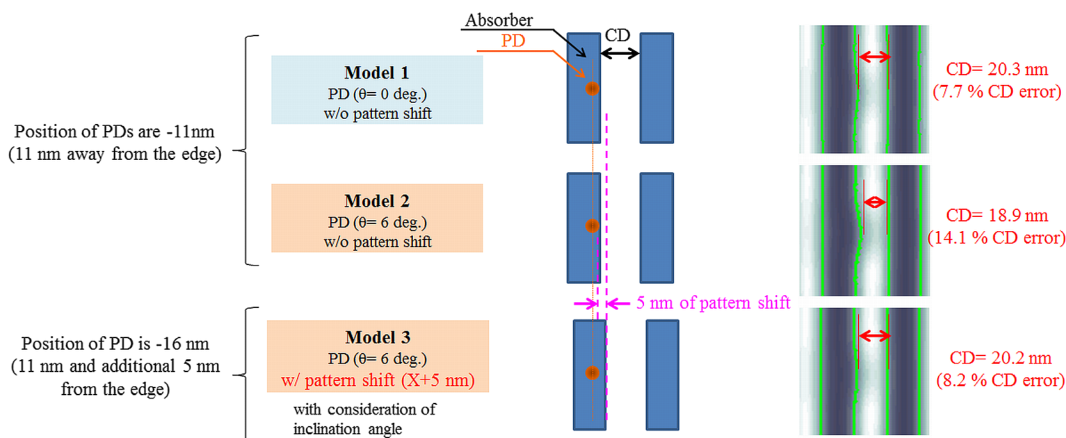

Fig. 13 Schematic view of the three kinds of calculation models for defect mitigation by shifting the absorber pattern and the calculated aerial image and CDs.

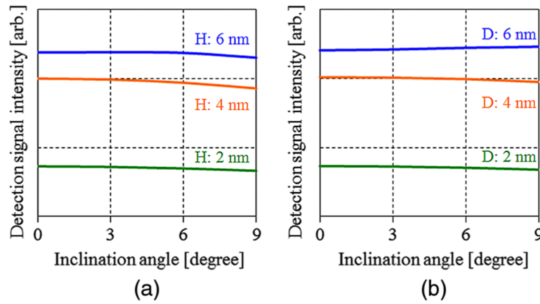

Fig. 14 Relationships between the inclination angle of PDs and the ABI defect detection signal intensity. The defect models are 2, 4, and 6 nm high and 50 nm wide, (a) bump and (b) pit.

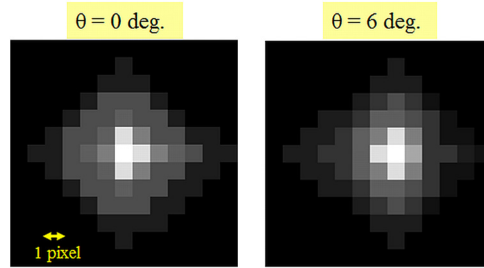

Fig. 16 Intensity level histogram of detection signal of ABI with high-magnification optics (20 nm/pixel).

3.5 *Impact of the Inclination Angle of Phase Defect on ABI Defect Detection Signal*

In this section, the impact of the inclination angle on the defect detection signal of an actinic inspection tool is described using the parameters for simulation described in Sec. 2.3. Regarding the PD detection signal intensity, the influences of the inclination angle of PDs on ABI detection signal intensity were negligibly small as shown in Fig. 14(a) and 14(b). Therefore, diagonal-type PDs are assumed to be detected by the ABI tool almost with the same detection sensitivity as the vertical-type would be. To pinpoint the position of PDs, the current ABI tool with a pixel size of 500 nm on mask seems to be insufficient to verify the position shift value caused by the inclination angle. To accurately pinpoint the position of both vertical and diagonal-type PDs, a smaller pixel size (e.g., 20 nm/pixel) was employed using high magnification inspection optics, as shown in Fig. 15. By employing a 20 nm pixel size, the calculated inspection signal intensity level histogram for vertical and diagonal-type bump-PDs (4 nm in height, 50 nm in width, and 0 deg or 6 deg in theta) was captured by the ABI tool and is shown in Fig. 16. The intensity histogram shows that the pixel position with peak intensity for diagonal-type PD with an inclination angle of 6 deg was shifted one pixel to the right side with respect to the pixel position with peak intensity for the vertical-type PD. Figure 17 shows the cross-section of the histogram shown in Fig. 16. The difference in the position of both PDs was calculated as 5.8 nm when the positions of the PDs were defined at half-maximum signal intensity. This result is in good agreement with the results of lithography simulation described in Sec. 3.4. Therefore, a dark-field ABI tool with a 20 nm pixel size has the capability to pinpoint the effective location of PDs and can give reliable information for defect mitigation.

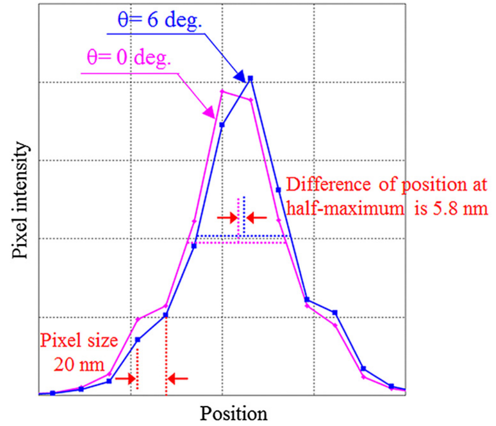

Fig. 17 Pixel intensity distribution for PD detection as the cross-section of Fig. 16.

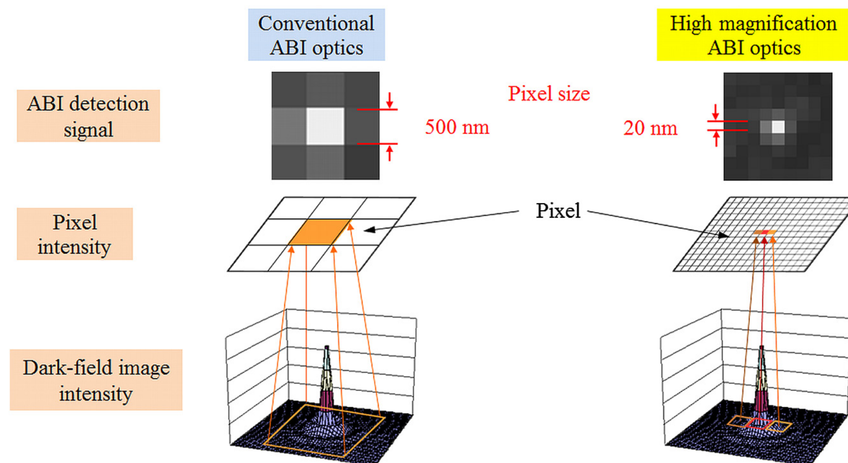

Fig. 15 Schematic view of the impact of pixel size on ABI detection signal. Large pixel size is due to low magnification optics while small pixel size will be achieved by using high magnification optics.

4 Summary

Diagonal-type PDs were observed by using TEM. The influences of the inclination angle, size, defect category (bump or pit), and positions of the PDs on defect printability were analyzed to study the effect of inclined-angle growth. As the inclination angle increased, the effective PD position shifted and became different from the PD position as defined by the multilayer surface topography. A PD with an inclination angle of 1 deg corresponded to a positional shift of one nanometer. The impact of the inclination angle on printing performance was quite noticeable when the PDs were not covered with the absorber pattern, and the impact must be understood accurately for defect mitigation by shifting the location of absorber patterns. The shifted effective PD position can be detected successfully by an ABI tool using high magnification optics without any noticeable signal intensity decrease due to a variation of PD's inclination angle. The positional shift of PDs induced by diagonal defect growth is detected by an ABI tool with the same magnitude that the image shift is seen by the exposure tool. The pattern-shifting strategies based on the information of the location of PDs provided by the ABI tool is reliable.

Acknowledgments

This work was supported by New Energy and Industrial Technology Development Organization.

References

1. T. Terasawa et al., "Phase defect printability and actinic dark-field mask blank inspection capability analyses," *Proc. SPIE* **7969**, 79690V (2011).
2. T. Terasawa et al., "Actinic phase defect detection and printability analysis for patterned EUVL mask," *Proc. SPIE* **7636**, 763602 (2010).
3. G. Zhang et al., "EUV mask readiness for high volume manufacturing," presented at *International Symposium on Extreme Ultraviolet Lithography 2010*, Sematech, Kobe, Japan (17–20 October 2010).
4. R. Jonckheere et al., "Progress forwards defect-free EUV reticles for NXE:3100," presented at *International Symposium on Extreme Ultraviolet Lithography 2011*, Sematech, Miami, Florida (17–19 October 2011).
5. H. Miyai, "EUV actinic blank inspection tool development," presented at *International Symposium on Extreme Ultraviolet Lithography 2011*, Sematech, Miami, Florida (17–19 October 2011).
6. T. Yamane et al., "Signal analysis for the actinic full-field EUVL mask blank inspection system," *Proc. SPIE* **7122**, 71222D (2008).
7. K. A. Goldberg et al., "Benchmarking EUV mask inspection beyond 0.25 NA," *Proc. SPIE* **7122**, 71222E (2008).
8. S. Perlitz et al., "Development status and infrastructure progress update of aerial imaging measurements on EUV masks," *Proc. SPIE* **8166**, 816610 (2011).

Tsuyoshi Amano received his BS and MS degrees in applied chemistry from Keio University in 1997 and 1999, respectively. He joined Dai Nippon Printing Co. Ltd., where he carried out research on mask process, metrology, and repair technology. In 2011, he was assigned to EIDEC, and since then he has been engaged in the development of patterned masks and blank inspection tools.

Biographies and photographs for other authors are not available.